Topological Magnetic Insulators with Corundum Structure

Jing Wang,[1,2] Rundong Li,[2] Shou-Cheng Zhang,[2] and Xiao-Liang Qi[3,2]

[1]*Department of Physics, Tsinghua University, Beijing 100084, China*

[2]*Department of Physics, McCullough Building, Stanford University, Stanford, California 94305-4045, USA*

[3]*Microsoft Research, Station Q, Elings Hall, University of California, Santa Barbara, California 93106, USA*

(Received 3 August 2010; published 24 March 2011)

Topological insulators are new states of quantum matter in which surface states residing in the bulk insulating gap are protected by time-reversal symmetry. When a proper kind of antiferromagnetic long-range order is established in a topological insulator, the system supports axionic excitations. In this Letter, we study theoretically the electronic states in a transition metal oxide of corundum structure, in which both spin-orbit interaction and electron-electron interaction play crucial roles. A tight-binding model analysis predicts that materials with this structure can be strong topological insulators. Because of the electron correlation, an antiferromagnetic order may develop, giving rise to a topological magnetic insulator phase with axionic excitations.

DOI: 10.1103/PhysRevLett.106.126403 PACS numbers: 71.70.Ej, 73.20.−r, 75.30.Kz, 75.80.+q

The discovery of a time-reversal invariant (TRI) topological insulator (TI) has attracted a great deal of attention in condensed matter physics [1–9]. With time-reversal symmetry $\mathcal{T}$ broken on the surface, the electromagnetic response of three-dimensional (3D) insulators is described by the topological θ term of the form $S_\theta = (\theta/2\pi) \times (\alpha/2\pi) \int d^3x dt \mathbf{E} \cdot \mathbf{B}$ together with the ordinary Maxwell terms, where $\mathbf{E}$ and $\mathbf{B}$ are the conventional electromagnetic fields inside the insulator, $\alpha = e^2/\hbar c$ is the fine structure constant, and θ is the dimensionless pseudoscalar parameter describing the insulator, which refers to the ''axion'' field in axion electrodynamics [10]. For a system without boundaries, all the physical quantities are invariant if θ is shifted by an integer multiple of 2π. Therefore, all TRI insulators fall into two distinct classes described by either $\theta = 0$ (trivial insulator) or $\theta = \pi$ (TI) [11]. Such a universal value of $\theta = \pi$ in TIs leads to a magnetoelectric effect with an universal coefficient, which has several unique experimental consequences such as a topological contribution to the Faraday and Kerr effect [11–13], and the image monopole induced by an electron [14]. θ has an explicit microscopic expression of the momentum space Chern-Simons form which depends on the band structure of the insulator [11]:

$$\theta = \frac{1}{4\pi} \int d^3k \epsilon^{ijk} \mathrm{Tr}\left[A_i \partial_j A_k + i \frac{2}{3} A_i A_j A_k \right], \quad (1)$$

where $A_i^{\mu\nu}(\mathbf{k}) = -i\langle u_\mu | \partial/\partial k_i | u_\nu \rangle$ is the momentum space non-Abelian gauge field, with $|u_\mu\rangle$ and $|u_\nu\rangle$ referring to the Bloch wave function of occupied bands.

If a strong electron correlation exists in a TI, a long-range antiferromagnetic order can be established under a low enough temperature. Since the antiferromagnetic order breaks $\mathcal{T}$ spontaneously, θ can deviate from π and also becomes a *dynamical* field which has fluctuations associated with some spin collective modes. Such a nonconventional antiferromagnetic insulator supporting axion excitations is proposed as a topological magnetic insulator (TMI) [15]. Because of its coupling to photons, the axion field hybridizes with photons, leading to an axion polariton, with a polariton gap tunable by an external magnetic field. Thus such a material can be used as a novel type of optical modulator to control the transmission of light through the material.

To realize the TMI phase, we need both the nontrivial topology of the electron bands and a strong electron correlation. The materials with electrons in the $3d$, $4d$, or $5d$ orbital can have both strong spin-orbit coupling (SOC) and strong interaction, which is ideal for this purpose. Recently, models for TIs with a strong electron correlation have been proposed [16–19]; also, topological phases may exist in thallium-based III-V-VI_2 ternary chalcogenides [20] as well as ternary Heusler compounds [21,22]. In this Letter, we study theoretically the transition metal oxide ABO_3 of corundum structure with A and B standing for some transition metals such as Fe, Ru, Rh, Ir, Os, etc. [23]. A possible candidate material is α-Fe_2O_3. A tight-binding model is obtained by using the point group symmetry of this structure, from which we find a TMI phase with a certain SOC strength and electron-electron interaction.

The corundum structure is shown in Fig. 1(a). Each transition metal atom is surrounded by an oxygen octahedron, and the d orbitals are split by the octahedral crystalline field into doublet $e_g(x^2 - y^2, 3z^2 - r^2)$ and triplet $t_{2g}(xy, yz, zx)$ orbitals [see Fig. 1(c)]. We will neglect a small distortion of the oxygen octahedra which may lead to minor corrections to the electronic structure [24]. The energy of t_{2g} stays lower with respect to e_g, because the latter point towards the negatively charged oxygens. The SOC is effective in t_{2g} orbitals and negligible in e_g orbitals. Including the SOC, t_{2g} splits into total angular

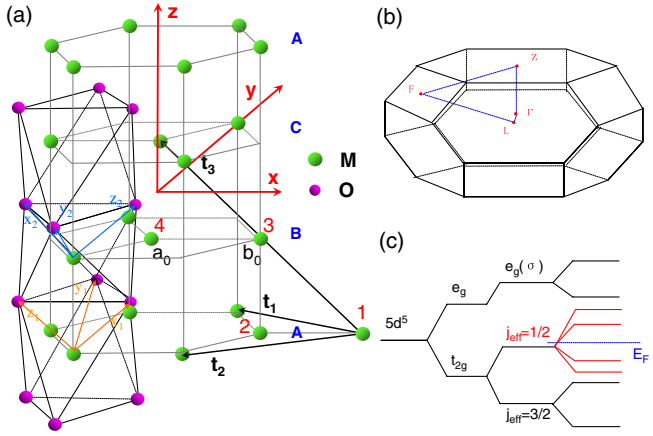

FIG. 1 (color online). (a) Corundum crystal structure with three primitive lattice vectors denoted as $\vec{t}_{1,2,3}$. Each transition metal ion M ($M =$ Ir, Os, etc.) (green large circles) is surrounded by oxygen octahedron (red small circles). (b) Brillouin zone for corundum structure. The four inequivalent TRI points are $\Gamma(000)$, $F(\pi 00)$, $L(\pi\pi\pi)$, and $Z(00\pi)$. (c) Schematic crystal field splitting of the $5d$ level in a corundum structure. We are interested in the half filling case with effective angular momentum $j_{\text{eff}} = 1/2$.

momentum $j_{\text{eff}} = 3/2$ and $j_{\text{eff}} = 1/2$. We focus on those materials where the Fermi level lies completely in the $j_{\text{eff}} = 1/2$ subbands. For example, the ions Fe^{3+}, Ir^{4+}, etc. with five d electrons satisfy this requirement [23].

To obtain the electron dynamics in this system, we start with a symmetry analysis to the corundum structure. The space group of this structure is $D_{3d}^5(R\bar{3}c)$. It has a trigonal axis (threefold rotation symmetry C_3) defined by the z axis, a binary axis (twofold rotation symmetry C_2), defined by the y axis, and inversion symmetry with the inversion center at the middle of the two neighbor transition metal atoms. The primitive lattice vectors $\vec{t}_{1,2,3}$ and primitive unit cells are shown in Fig. 1(a), where each unit cell consists of four transition metal atoms denoted as 1, 2, 3, and 4. Since the oxygen p-level ϵ_p are far away from the Fermi level, we can consider a model describing only d electrons, with the hopping mediated by the oxygen p orbitals. The model is generally written as

$$\mathcal{H}_0 = -\sum_{\langle ij\rangle}[d_i^\dagger t_{ij} d_j + \text{H.c.}] + \sum_{\langle\langle ij\rangle\rangle}[d_i^\dagger \hat{t}'_{ij} d_j + \text{H.c.}], \quad (2)$$

where $\langle ij\rangle$ and $\langle\langle ij\rangle\rangle$ denote the nearest-neighbor (NN) and next-nearest-neighbor (NNN) sites, respectively, and the hopping terms t_{ij} and $\hat{t}'_{ij}$ are in general 2×2 matrices. The form of the parameters t_{ij} and $\hat{t}'_{ij}$ can be simplified by symmetry considerations. Because of space limitation, we will present only the result of the symmetry analysis. The NN transfer integrals t_{ij} are real and spin-independent, with two independent parameters, the intraplane hopping t and the interplane hopping $t_\perp$. $t = (pd\pi)^2[(pp\sigma)+3(pp\pi)]/3(\epsilon_d - \epsilon_p)^2$ [17], where $(pd\pi)$, $(pp\sigma)$, and $(pp\pi)$ are Slater-Koster parameters between pd and pp, respectively [25]. The contribution of the order of $(pd\pi)^2/(\epsilon_d - \epsilon_p)$ cancels out in the honeycomb lattice, in sharp contrast to Sr_2IrO_4 with the perovskite lattice [26,27]. The NNN transfer integrals are spin-dependent, and they are essential for the realization of the TI phase. For the intraplane in layer A, $1 \to 1$ hopping can be written as

$$\hat{t}'_{11} = it'_{1\|}\vec{\sigma}\cdot\vec{r}_{11} + t_{1\|}, \quad (3)$$

where $\vec{r}_{11}$ is a unit vector $\vec{r}_{11} \propto \vec{t}_{11} + 1/\sqrt{2}\hat{z}$, $\vec{t}_{11}$ is the hopping link, and $\hat{t}'_{22} = \hat{t}'^{\dagger}_{11}$ due to inversion symmetry, while in the B plane, $\hat{t}'_{33} = e^{-i\pi/2\sigma_z}\hat{t}'_{11}e^{i\pi/2\sigma_z}$ and $\hat{t}'_{44} = e^{-i\pi/2\sigma_z}\hat{t}'_{22}e^{i\pi/2\sigma_z}$ due to C_2 symmetry. For the interplane ($A \to B$),

$$\hat{t}'_{13} = it'_{2\perp}\vec{\sigma}\cdot\vec{r}_{13} + t_{2\perp}, \quad (4)$$

where $\vec{r}_{13}$ is a unit vector $\vec{r}_{13} \propto \vec{t}_{13} - \alpha\hat{z}$, $\vec{t}_{13}$ is the hopping link, and α is some parameter which depends on materials and cannot be determined purely by symmetry; below, we choose $\alpha = 1/\sqrt{2}$, which has almost the same amplitude as the intraplane. $\hat{t}'_{24} = \hat{t}'_{13}$ and $\hat{t}'_{14} = \hat{t}'_{23} = e^{-i\pi/6\sigma_z}\hat{t}'_{13}e^{i\pi/6\sigma_z}$. Explicitly, $\vec{r}_{ij}$ for the intraplane $1 \to 1$, $2 \to 2$ hopping are x_1, y_1, and z_1 and for $3 \to 3$, $4 \to 4$ are x_2, y_2, and z_2 denoted in Fig. 1(a).

In summary, the transfer integrals are real and spin-independent for NN links but complex and spin-dependent for NNN links. The accurate hopping parameters vary in different materials. As an example, in the following we will use the transfer integrals of Ir oxide introduced in Ref. [17]. One can always define all the parameters in the unit of in-plane NN hopping t, which leads to $t = 1$, $t'_{1\|} = 0.33$, $t_{1\|} = -0.1$, $t_\perp = y$, $t_{2\perp} = 0.5y$, and $t'_{2\perp} = \lambda t_{2\perp} = 0.4y$. Here λ is the SOC strength which determines the ratio of spin-dependent hopping and spin-independent hopping. For Ir oxide we have $\lambda = 0.8$. All the interplane hopping matrix elements are rescaled by a factor y which incorporates the anisotropy between intraplane and interplane directions. The energy dispersions for $y = 0.3$ (dashed line) and $y = 0.55$ (solid line) are shown in Fig. 2(a), which shows that the system at half filling is an insulator in both cases. Because of inversion symmetry, all the energy bands are doubly degenerate.

In 3D TIs, four independent Z_2 topological invariants can be defined [28–30]. For inversion symmetric systems, all the topological invariants can be simply determined by the parity of the wave functions at the 8 TRI momenta (TRIM) in the Brillouin zone [3]. $\mathbf{G}_1$, $\mathbf{G}_2$, and $\mathbf{G}_3$ are the three basis vectors of the reciprocal lattice; then the 8 TRIM are defined by $\mathbf{k}_i = (k_1\mathbf{G}_1 + k_2\mathbf{G}_2 + k_3\mathbf{G}_3)/2\pi$ with $k_1, k_2, k_3 = 0$ or π. For each TRIM $\mathbf{k}_i$, one can define a Z_2 quantity δ_i as the multiplication of the parity of all occupied bands $\delta_i = \prod_{s\in\text{occ}}\xi_s$, with ξ_s the parity of the sth band. It should be noticed that a Kramers pair of bands

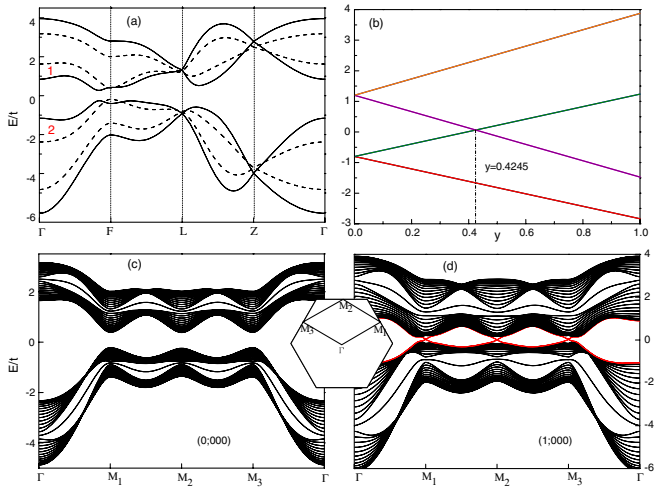

FIG. 2 (color online). (a) 3D energy band dispersion of tight-binding model for a corundum structure with $\lambda = 0.8$ and $y = 0.3$ (dashed line) and $y = 0.55$ (solid line). (b) The change of energy levels at F point ($\pi 00$) versus y. A band crossing occurs at $y = 0.4245$. The system changes from a trivial insulator to a TI. (c),(d) 2D band structure for a slab with 001 surface for the parameters $\lambda = 0.8$ and $y = 0.3$ in (c) and $y = 0.55$ in (d). The red curves in (d) stand for surface states. The inset shows the surface Brillouin zone.

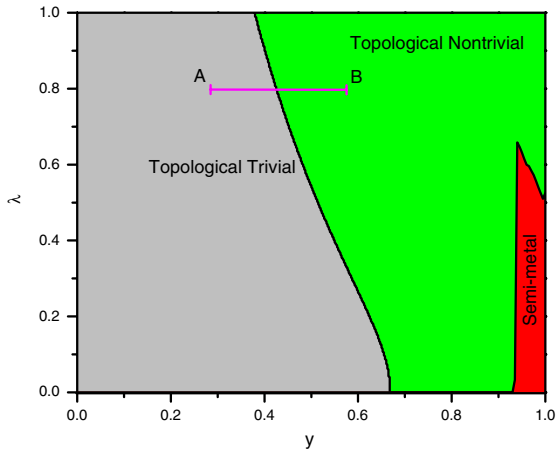

FIG. 3 (color online). The phase diagram of the system with two variables: the anisotropy parameter y and SOC parameter λ. The green and gray regions stand for topological nontrivial and trivial phases, respectively. Points A and B correspond to the parameters used in Figs. 2(c) and 2(d), respectively.

are counted only once; otherwise, δ_i would always be even. The four Z_2 invariants $(\nu_0; \nu_1\nu_2\nu_3)$ can be determined by δ_i in which $\nu_0 = \prod_{i=1}^{8} \delta_i$ is the strong topological invariant. For $y = 0.3$, we find $\delta = +1$ at all TRIM at half filling. On the contrary, for $y = 0.55$ we find $\delta = -1$ at the three F points [see Fig. 1(b)] and $\delta = +1$ at all other TRIM. Consequently, the $y = 0.55$ phase is a strong TI with the topological character (1; 000), and $y = 0.3$ is a trivial insulator with character (0; 000). From this result we see that a band inversion [1] occurs at F points upon the change of y. In Fig. 2(b), we show the energy at F point versus y, from which one can see clearly a level crossing at $y \simeq 0.42$. The topological invariants can be calculated for all values of anisotropy parameter y and SOC parameter λ, which leads to the phase diagram shown in Fig. 3. One can see that the topological nontrivial band structure can be realized at large y (i.e., small anisotropy) even for infinitesimal SOC. However, one should notice that for some parameters the band structure is actually a semimetal (similar to Sb), which has a direct gap but does not have an indirect gap. We also solve the Hamiltonian (2) in a slab geometry with two 001 surfaces to study explicitly the topological surface states. Figures 2(c) and 2(d) show the 2D energy dispersion of the two systems shown in Fig. 2(a). In addition to the bulk states, for $y = 0.55$ there are surface states with three Dirac cones at M points of the surface Brillouin zone, while no surface state is found for $y = 0.3$, in consistency with the bulk topological invariants.

To get a better understanding of the physical properties of this system, a low energy effective model can be obtained by expanding the Hamiltonian around the F points. Around each F point, the effective model is 4×4 which describes two Kramers pairs of low lying bands and has Dirac-like form. In the following, we will denote the momentum by its coordinate in the basis of reciprocal lattice, i.e., $\mathbf{k} = (k_1\mathbf{G}_1 + k_2\mathbf{G}_2 + k_3\mathbf{G}_3)/2\pi$. The F points are given by $(\pi, 0, 0)$, $(0, \pi, 0)$, and $(\pi, \pi, 0)$. Around the point $(\pi, 0, 0)$ the Hamiltonian has the following form:

$$\mathcal{H}_{\text{eff}}(\pi 00) = \epsilon_0(\mathbf{q})\mathbb{I}_{4\times 4} + \sum_{a=1}^{5} d_a(\mathbf{q})\Gamma_a. \qquad (5)$$

Here the Dirac Γ matrices are defined as $\Gamma_a = (\tau_x \otimes \sigma_x, \tau_x \otimes \sigma_y, \tau_y \otimes 1, \tau_z \otimes 1, \tau_x \otimes \sigma_z)$, where τ_i and σ_i $(i = x, y, z)$ denote the Pauli matrices in the space of orbital and spin, respectively. $\mathbf{q} = \mathbf{k} - (\pi 00)$, $d_a(\mathbf{q}) = \sum_{i=1,2,3} A_i^a q_i$ for $a = 1, 2, 3, 5$, $d_4(\mathbf{q}) = M + \sum_{i=1,2,3} B_i q_i^2$, and $\epsilon_0(\mathbf{q}) = C + \sum_{i=1,2,3} D_i q_i^2$. For $\lambda = 0.8$, around the topological phase transition point we have

$$A_i^a = \begin{pmatrix} 0.14 & -0.12 & 0.37 & -0.34 \\ -0.47 & 0.06 & -0.13 & 0.09 \\ 0.014 & 0.038 & 0.015 & 0.055 \end{pmatrix},$$

$$B_i = (0.625, 0.32, 0.24), \qquad D_i = (0.375, 0.04, 0.04)$$

and $C = 0.064$. The mass parameter M depends on y as $M \approx -23y + 9.76$, which changes sign at $y \simeq 0.42$ and leads to the topological phase transition. The effective Hamiltonian around the other two F points at $(0\pi 0)$ and $(\pi\pi 0)$ can be obtained by C_3 rotation.

Now we study the effect of electron correlation. The leading term in the interaction Hamiltonian is the on-site Hubbard repulsion for the $j_{\text{eff}} = 1/2$ orbitals $H_{\text{int}} = U\sum_i n_{i\uparrow} n_{i\downarrow}$. Magnetic ordering can be studied in the mean-field approximation. For simplicity, we consider

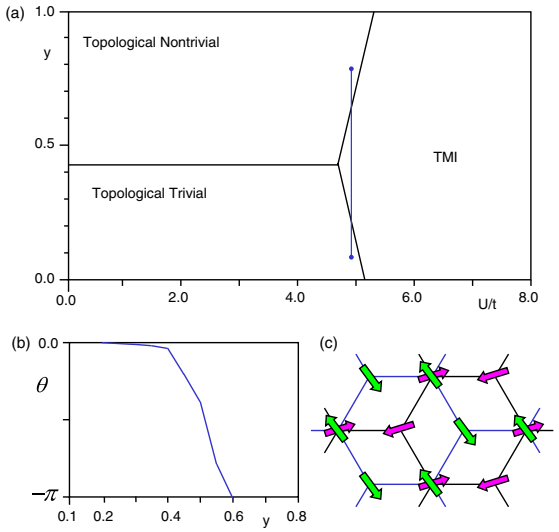

FIG. 4 (color online). (a) The phase diagram with y and U as parameters. (b) The value of θ along the blue line in the phase diagram. θ deviates from the TRI values 0 and π in the SDW phase. (c) The SDW order pattern. The purple arrows denote the spin in the A layer, and the green arrows denote the spin in the adjacent B layer. Other possible spin orderings can be obtained by sixfold rotations of this one.

only the order parameters that do not break translational symmetry. The mean-field calculation predicts a spin-density wave (SDW) phase above a critical U, and the spin moments of this SDW phase lie in the honeycomb plane, which are ordered antiferromagnetically within each layer and noncollinear between the two neighboring layers, as shown in Fig. 4. A finite mass for exciting the SDW phase is, for example, $m_{\mathrm{SDW}}/t = 3.65$ when $U/t = 6.0$. Experimentally, α-Fe_2O_3 develops a canted antiferromagnetic phase with spins residing in the honeycomb layer when $T_M < T < T_{\mathrm{Néel}}$, where T_M is the Morin transition temperature [31–33]. Spins in each layer are parallel, and those in two adjacent layers are coupled antiferromagnetically. Moreover, due to a slight spin canting, the spins in adjacent layers are not exactly antiparallel (noncollinear). Spins can be ordered along one of three directions interchanged by C_3 and are homogeneously distributed in the crystal [31,32]. The deviation from the SDW pattern may due to the hopping parameters chosen in the calculation [33]. Although it is different from the pattern we obtained in Fig. 4, the spin ordering in bulk α-Fe_2O_3 breaks $\mathcal{T}$, giving rise to $\theta \neq 0, \pi$. Therefore, α-Fe_2O_3 is a possible material to realize TMI.

The value of θ in the SDW phase of this effective model can be calculated as in Ref. [15]:

$$\theta = \frac{1}{4\pi}\int d^3k \frac{2|d| + d_4}{(|d| + d_4)^2|d|^3}\epsilon^{ijkl} d_i \partial_x d_j \partial_y d_k \partial_z d_l, \quad (6)$$

where $i, j, k, l = 1, 2, 3, 5$ and $|d| = (\sum_{a=1}^{5} d_a^2)^{1/2}$. Since the main contribution to θ comes from the region close to Dirac points, θ can be approximated by the sum of θ's calculated separately for each Dirac point by using the effective model. The numerical results of θ is shown in Fig. 4(b).

We thank T. L. Hughes, Ian Fisher, Z. J. Xu, and B. F. Zhu for insightful discussion. This work is supported by the NSF under Grant No. DMR-0904264 and by the Keck Foundation. J. W. acknowledges the support of China Scholarship Council, NSF of China (Grant No. 11074143), and the Program of Basic Research Development of China (Grant No. 2011CB921901).

[1] B. A. Bernevig, T. L. Hughes, and S. C. Zhang, Science **314**, 1757 (2006).
[2] M. König *et al.*, Science **318**, 766 (2007).
[3] L. Fu and C. L. Kane, Phys. Rev. B **76**, 045302 (2007).
[4] D. Hsieh *et al.*, Nature (London) **452**, 970 (2008).
[5] H. Zhang *et al.*, Nature Phys. **5**, 438 (2009).
[6] Y. Xia *et al.*, Nature Phys. **5**, 398 (2009).
[7] Y. L. Chen *et al.*, Science **325**, 178 (2009).
[8] X. L. Qi and S. C. Zhang, Phys. Today **63**, No. 1, 33 (2010).
[9] M. Z. Hasan and C. L. Kane, Rev. Mod. Phys. **82**, 3045 (2010).
[10] F. Wilczek, Phys. Rev. Lett. **58**, 1799 (1987).
[11] X. L. Qi, T. L. Hughes, and S. C. Zhang, Phys. Rev. B **78**, 195424 (2008).
[12] W. K. Tse and A. H. MacDonald, Phys. Rev. Lett. **105**, 057401 (2010).
[13] J. Maciejko *et al.*, Phys. Rev. Lett. **105**, 166803 (2010).
[14] X. L. Qi *et al.*, Science **323**, 1184 (2009).
[15] R. Li *et al.*, Nature Phys. **6**, 284 (2010).
[16] S. Raghu *et al.*, Phys. Rev. Lett. **100**, 156401 (2008).
[17] A. Shitade *et al.*, Phys. Rev. Lett. **102**, 256403 (2009).
[18] H. M. Guo and M. Franz, Phys. Rev. Lett. **103**, 206805 (2009).
[19] D. Pesin and L. Balents, Nature Phys. **6**, 376 (2010).
[20] Y. L. Chen *et al.*, Phys. Rev. Lett. **105**, 266401 (2010).
[21] S. Chadov *et al.*, Nature Mater. **9**, 541 (2010).
[22] H. Lin *et al.*, Nature Mater. **9**, 546 (2010).
[23] C. T. Prewitt *et al.*, Inorg. Chem. **8**, 1985 (1969).
[24] I. Nebenzahl and M. Weger, Philos. Mag. **24**, 1119 (1971).
[25] W. A. Harrison, *Elementary Electronic Structure* (World Scientific, Singapore, 1999).
[26] B. J. Kim *et al.*, Phys. Rev. Lett. **101**, 076402 (2008).
[27] B. J. Kim *et al.*, Science **323**, 1329 (2009).
[28] J. E. Moore and L. Balents, Phys. Rev. B **75**, 121306 (2007).
[29] L. Fu, C. L. Kane, and E. J. Mele, Phys. Rev. Lett. **98**, 106803 (2007).
[30] R. Roy, Phys. Rev. B **79**, 195322 (2009).
[31] M. Brunel and F. De Bergevin, Acta Crystallogr. Sect. A **37**, 324 (1981).
[32] A. H. Morrish, *Canted Antiferromagnetism: Hermatite* (World Scientific, Singapore, 1994).
[33] M. Catti, G. Valerio, and R. Dovesi, Phys. Rev. B **51**, 7441 (1995).